

Tensile drawing behaviour of poly(ethylene terephthalate)

F. Rietsch†, R. A. Duckett and I. M. Ward

Department of Physics, University of Leeds, Leeds LS2 9JT, UK

(Received 6 February 1979; revised 17 May 1979)

A detailed study has been undertaken of the drawing behaviour of poly(ethylene terephthalate) over the temperature range 20° to 80°C. Cold drawing behaviour was observed at the lower temperatures and homogeneous deformation at 80°C. Samples were also subjected to two-stage drawing: homogeneous draw at 80°C followed by cold drawing at 20°C. In all cases the geometry of the deformation was monitored by measuring the changes in macroscopic dimensions. In addition, measurements were made of the final birefringence, and the shrinkage force developed when the drawn samples were heated to a temperature above T_g . The results are discussed in terms of continuum models for the deformation of polymers. In particular, the relevance of a simple molecular network model is considered. It is shown that many of the observations are consistent with the deformation of a molecular network, although our understanding of the molecular processes involved in cold drawing is still incomplete.

INTRODUCTION

In a previous paper¹, measurements of shrinkage force and birefringence for oriented poly(ethylene terephthalate) (PET) fibres have been described. The fibres were prepared by a fibre melt spinning process in which polymer is extruded through a small orifice (the spinneret) and the resultant thread (the spun yarn) allowed to cool in air before collection on a rotating drum (the wind-up). By varying the speed of rotation of the wind-up drum it was possible to obtain spun yarns with different degrees of molecular orientation. In this way a set of spun yarns was prepared with no crystallinity, and birefringences varying from almost zero to about 10^{-2} . When these yarns were heated to temperatures above the glass transition temperature T_g they showed marked shrinkage and an appreciable shrinkage force. Detailed measurements of birefringence, shrinkage and shrinkage force suggested that the spun yarn could be regarded as a stretched rubber network, with physical molecular entanglements as the network junction points, which was frozen when the threadline cooled rapidly. There was a constant stress optical coefficient C , relating the birefringence Δn and the shrinkage stress σ through $C = \Delta n/\sigma$, even when both Δn and σ decayed due to the breakdown of the molecular network, as the physical entanglements became free on continued heating above T_g . Moreover, σ and Δn related to the shrinkage s in a manner consistent with the simple molecular theory of rubber elasticity. We have:

$$\Delta n = C\sigma = NkTC(\lambda^2 - \lambda^{-1}) = NkTC \{(1 - s)^{-2} - (1 - s)\}$$

where the extension ratio of the network λ , relates to the measured shrinkage by the equation:

†Present address: Université des Science et Techniques de Lille, U.E.R. de Chimie, BP 36, 59-650 Villeneuve D'Ascq, France.

$$s = \frac{\lambda - 1}{\lambda}$$

and N is the number of molecular chains per unit volume.

A disadvantage of the previous studies was that the deformation of the PET took place under conditions where the imposed deformation, temperature and strain rate could not be defined. It was therefore of interest to deform PET under controlled conditions above T_g , and measure the birefringence and shrinkage stress as a function of the imposed extension ratio λ .

In addition to the examination of samples drawn above T_g , similar measurements have also been undertaken on samples drawn below T_g . Such samples cold draw through a neck to a 'natural' draw ratio, i.e. a limiting, constant degree of plastic deformation. This part of the investigation links with previous studies of cold drawing of PET fibres²⁻⁴ and especially with the finding that the natural draw ratio falls rapidly with increasing preorientation in the polymer before drawing. It has been proposed that this effect can be attributed to the existence of a molecular network with a limiting extensibility, which is independent of the division of extension between the extrusion (spinning) and drawing processes. Shrinkage force measurements have now been made on such samples in an attempt to confirm the validity of the molecular network hypothesis and, if possible, throw further light on its nature.

EXPERIMENTAL

Material

The samples studied were all taken from a film of amorphous PET supplied by ICI Ltd, Plastics Division, UK. The film was approximately 0.25 mm thick and was characterized by a low initial birefringence ($<0.4 \times 10^{-3}$) and a molecular weight of approximately 14 000 as determined by measurement of intrinsic viscosity. Samples were cut in

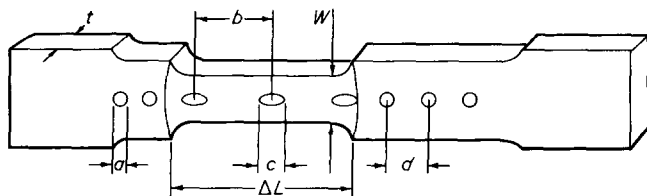


Figure 1 Schematic diagram illustrating the measurements made to calculate the draw ratios in a sample containing a neck, length ΔL .

	a/mm	b/mm	c/mm	d/mm
Initially isotropic	0.2	0.5λ	0.2λ	0.5
Two-stage drawn	$0.2\lambda_p$	0.5λ	0.2λ	$0.5\lambda_p$

the form of dumb-bells with straight gauge length 4.75×20 mm.

Drawing procedure

Each sample was marked along its centre line with a series of circular ink spots 0.2 mm in diameter equispaced at a distance of 0.5 mm to facilitate strain measurement. It was then stored in the environmental chamber of a conventional Instron machine for a period of 20 min to achieve thermal equilibrium at the test temperature.

Hot drawing. Most samples were deformed at 80°C at a constant crosshead speed of 0.125 cm min^{-1} , (a speed low enough to ensure isothermal conditions). After drawing for a predetermined time the crosshead was stopped and the sample was cooled quickly to below the glass transition temperature ($T_g \sim 68^\circ\text{C}$) using the cooling facility of the environmental chamber. On unloading, the samples had a residual deformation in the range $1.02 < \lambda_p < 4.6$, depending on the drawing time. (See below for details of strain measurements.)

A few additional drawing experiments were made using the higher crosshead speeds of 0.05 and 5 cm min^{-1} . In these experiments the recorded load–elongation curves were analysed to define the effective modulus at each drawing rate.

Cold drawing. A series of samples was deformed at the temperatures 20° , 40° and 60°C , the extent of draw being determined by the length ΔL of the well-defined neck observed in each case. The majority of samples were drawn at a crosshead speed of 0.125 cm min^{-1} with a smaller number using crosshead speeds in the range 0.05 to 1.25 cm min^{-1} .

Two-stage drawing. These samples were prepared in two successive stages: a homogeneous 'preorientation' at 80°C as described in (a) above, followed by 'cold drawing' at 20°C at a speed of 0.125 cm min^{-1} .

Strain measurement

The typical geometry of a neck in a cold drawn sample is shown schematically in Figure 1, which also indicates how measurements of the distortion of the printed ink spots, made with a micrometer eyepiece, lead to values for the draw ratio in each specimen. These measurements were supported by measurements of width w and thickness t using suitable micrometers and the calibrated focussing mechanism of a microscope in order to build up a comprehensive picture of the distribution of strain in each specimen.

Birefringence measurements

The measurements of optical retardation, all at ambient temperature, were made using an Ehringhaus calcite compensator in conjunction with a Zeiss polarizing microscope. These were combined with the measured thickness to calculate the birefringence of the samples point to point. This method of birefringence measurement was chosen in preference to the more accurate methods using immersion liquids because of the need to measure each sample before and after the shrinkage force measurement. Other work suggests that the systematic errors introduced are less than 10% and do not materially affect the conclusions drawn from this work.

Shrinkage force measurement

The apparatus constructed for shrinkage force measurement is shown in Figure 2. The sample A was constrained by grips B between an Instron load cell C (maximum force, 20N) and a crosshead D which could be positioned using screw E. The sample was surrounded by an enclosure F made from polyurethane foam to facilitate temperature control. This was achieved by passing compressed air past a loosely wound heater coil G of low thermal inertia, supplied with electrical power from a Eurotherm temperature controller operating from a copper–constantan thermocouple.

Measurements were made by inserting a sample between the grips and adjusting the screw E to impart a small tension. The temperature controller was then switched on to produce a rapid increase in sample temperature to 87°C and then subsequent control at that temperature with minimal oscillations. The temperature of 87°C was chosen to be sufficiently above the glass transition but still below the temperature at which isotropic PET is generally believed to crystallize. It was possible with this apparatus to heat the sample from 20° to 68°C within 20 s and to achieve a constant temperature of 87°C in 40 s.

RESULTS

General aspects of drawing behaviour

There was a dramatic change in the nature of the drawing behaviour in the vicinity of the glass transition tem-

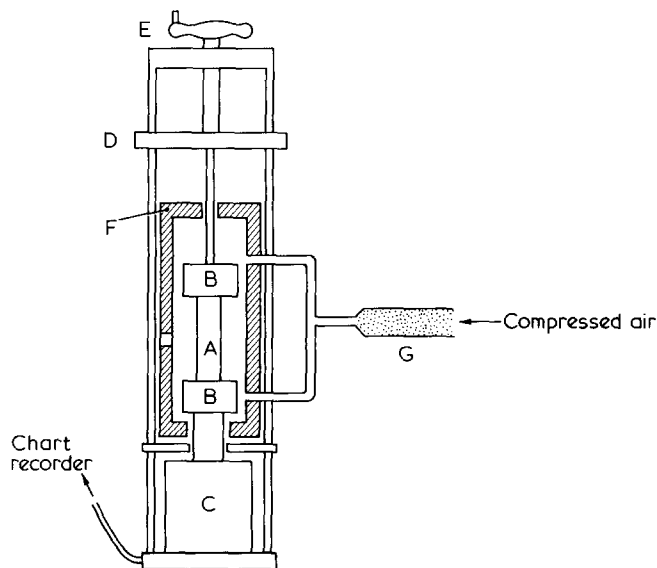


Figure 2 Shrinkage force apparatus, see text

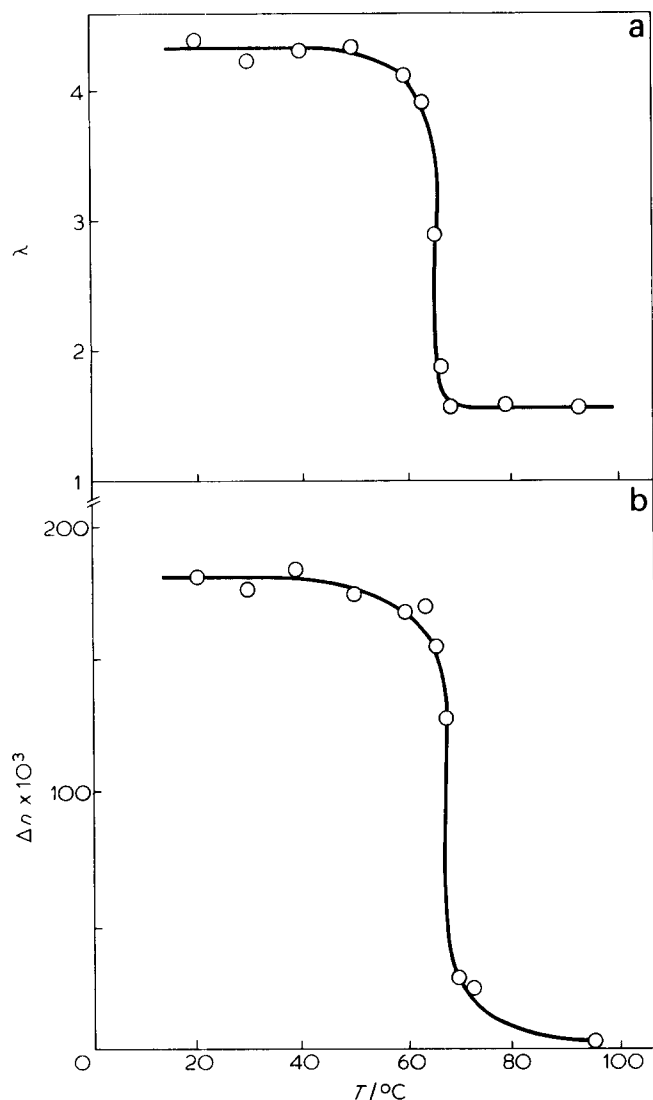


Figure 3 Variation of (a) draw ratio λ and (b) birefringence Δn for samples drawn at different temperatures to a necklength $\Delta L = 12$ mm

perature. This is illustrated in Figures 3a and 3b, which show the natural draw ratio, λ_N , and birefringence, Δn , in the centre of a neck as a function of drawing temperature for a series of samples drawn to $\Delta L = 12$ mm. At temperatures less than 60°C the sample necked sharply down to a constant draw ratio of approximately 4.3. Necks formed at higher temperatures became more diffuse until above T_g the sample deformed homogeneously to a draw ratio defined by the overall deformation. This sudden change in deformation behaviour was also reflected in the birefringence which is shown in Figure 3b.

Neck geometry

Figure 1 typifies a specimen at an intermediate stage of cold draw, and indicates the dimensional changes of interest here. Dimensional measurements and birefringence measurements on necks in a large number of specimens are summarized in Figures 4, 5, 6 and 7. Figure 4 shows detailed measurements on the geometry of a neck and the birefringence in a specimen drawn at 20°C to a total neck length $\Delta L = 12$ mm. Figures 4a and 4b show the variations, point by point, in birefringence and thickness, respectively, across the width at different distances Δy from the shoulder

of a neck grown to a total length of $\Delta L = 23$ mm, and therefore indicate an inhomogeneity of strain within the neck. Figure 5 shows the variation of thickness and width at the centre of a neck for different neck lengths ΔL .

When thickness and width data were combined with measurements of the spacing and sizes of ink-marks it was possible to reconstruct the data in Figure 6 which show the variation in draw ratio and birefringence on the centre line of a neck along the specimen axis for necks of different lengths $\Delta L \sim 0.5, 4$ and 25 mm, all specimens 'cold-drawn' at 20°C. Figure 7 summarizes similar data from necks in specimens drawn to a constant length $\Delta L = 12$ mm at temperatures of 30°, 50°, 60°, 66° and 70°C. All subsequent birefringence and draw ratio data refer to measurements taken in the centre of the neck.

Birefringence data

Figure 8 shows the measured variation of birefringence Δn vs. $\lambda^2 - \lambda^{-1}$ for samples drawn at 80°C. (Note that the strain was homogeneous for drawing at this temperature.) Birefringence data from the central regions of necks

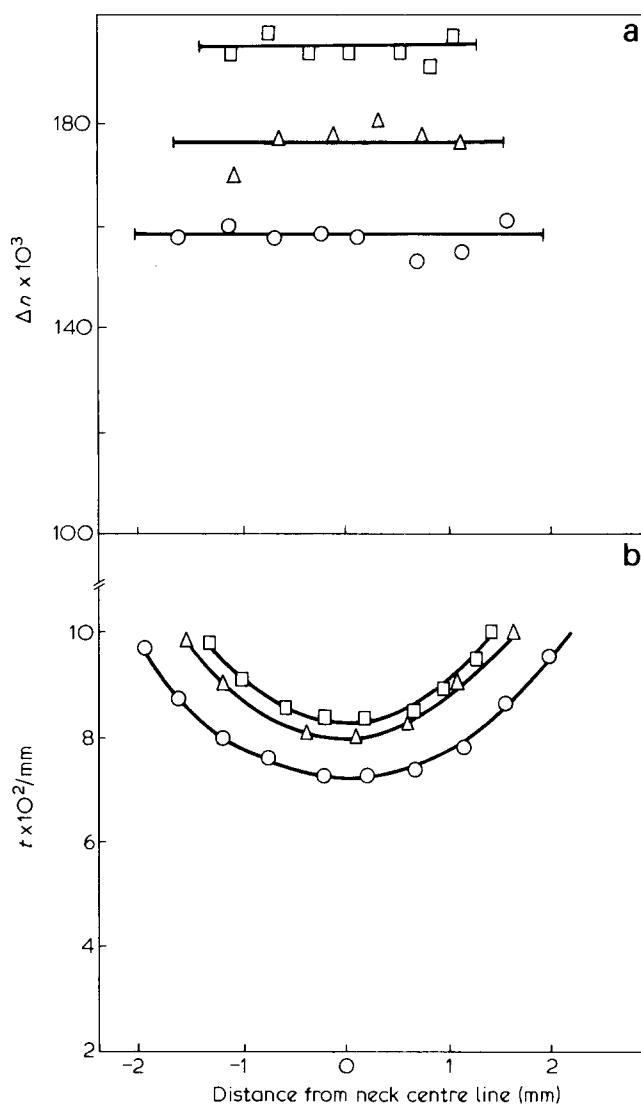


Figure 4 (a) Variation of birefringence across the width of a neck in a sample drawn to $\Delta L = 23$ mm at 20°C. Distance from shoulder (mm) \circ , 0.55; \triangle , 3.2; \square , 11.5. (b) Variation of thickness across the width of the same specimen as in (a). Symbols have the same significance

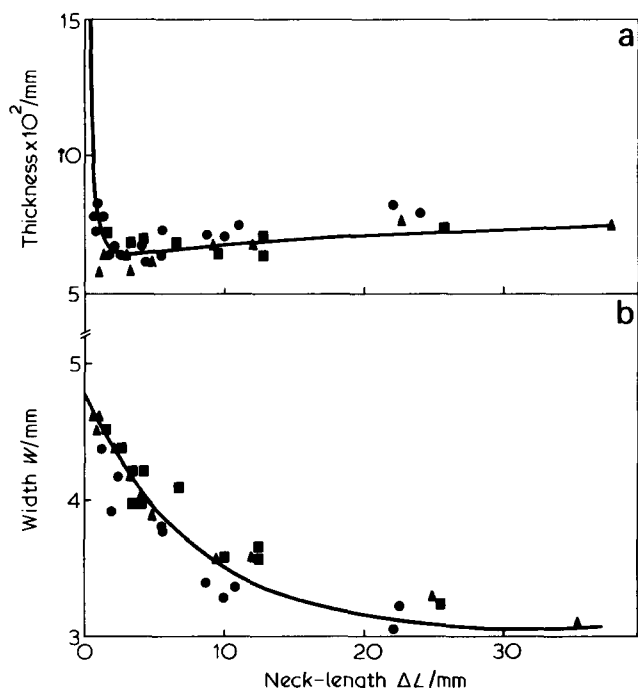


Figure 5 (a) Variation of thickness, t , at midpoint of neck versus neck length, ΔL . (b) Variation of width, w , at midpoint of neck versus neck length, ΔL . \bullet , $T = 20^\circ\text{C}$; \blacktriangle , $T = 40^\circ\text{C}$; \blacksquare , $T = 60^\circ\text{C}$

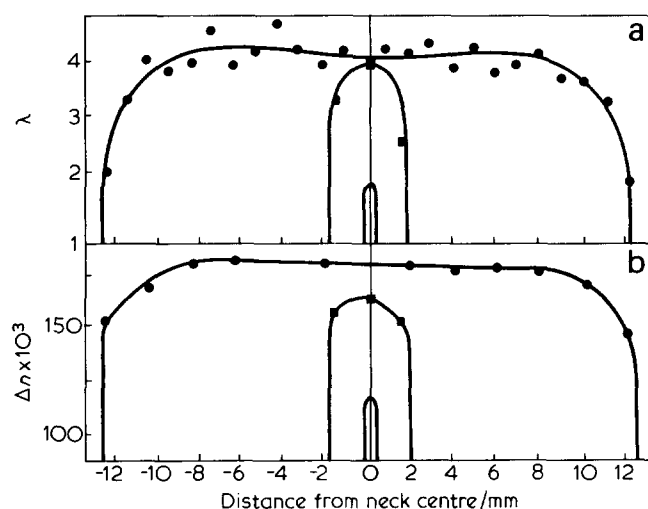


Figure 6 Variation of (a) draw ratio λ and (b) birefringence Δn along centre line of necks of different neck lengths: ΔL /mm = \blacktriangle , 0.44; \blacksquare , 4; \bullet , 24.5. $T = 20^\circ\text{C}$

in cold drawn samples (drawn at 20° , 40° and 60°C) are shown in Figure 9 also plotted as a function of $\lambda^2 - \lambda^{-1}$. The straight line relationship observed at 80°C in Figure 8 is added as a dashed line in Figure 9 to help comparisons between data from specimens drawn above and below the glass transition temperature.

Figure 10 shows the birefringence data from the two-stage drawing process plotted in the form of $\Delta n - \Delta n_p$ versus $(\lambda/\lambda_p)^2 - (\lambda_p/\lambda)$. Here Δn and Δn_p refer to the final birefringence and the birefringence after the initial preorientation stage, respectively; λ_p and λ refer to the draw ratio imposed in the preorientation stage and to the final draw ratio, and the combination λ/λ_p is equal to the 'natural draw ratio', λ_N , imposed at room temperature on the preoriented material.

Shrinkage force measurements

Representative shrinkage force measurements at a temperature of 87°C for samples with a range of draw ratios λ and drawing temperatures are shown in Figure 11. It is clear that there was, in general, a complex build up and decay of shrinkage force which varied systematically with the deformation and temperature history of the samples. As will be discussed below, only the initial peak has a ready interpretation and unless otherwise stated the term 'shrinkage stress' in what follows refers to the first (tensile) peak value of the shrinkage stress. The variation of this peak shrinkage stress with draw ratio is shown in Figure 12 for 'hot drawn' samples ($T_D = 80^\circ\text{C}$) and in Figure 13 for cold drawn ($T_D = 20^\circ$, 40° , 60°C) and two-stage drawn samples.

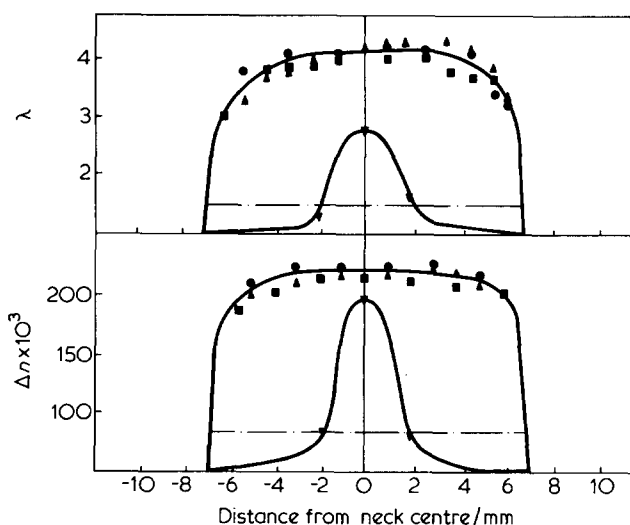


Figure 7 Variation of (a) draw ratio λ and (b) birefringence Δn along centre line of necks. $\Delta L = 12$ mm, drawn at $T^\circ\text{C} = \bullet$, 30; \blacktriangle , 50; \blacksquare , 60; \blacktriangledown , 66; — — — homogeneous draw at 70°C

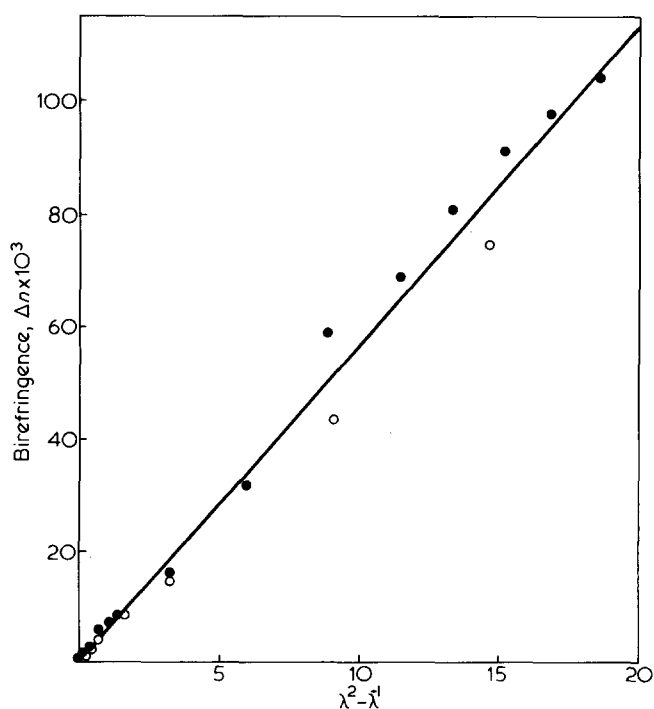


Figure 8 Plot of birefringence $\Delta n \times 10^3$ vs. $\lambda^2 - \lambda^{-1}$ for samples drawn at 80°C . Crosshead speed: \bullet , 0.5 cm/min; \circ , 0.125 cm/min

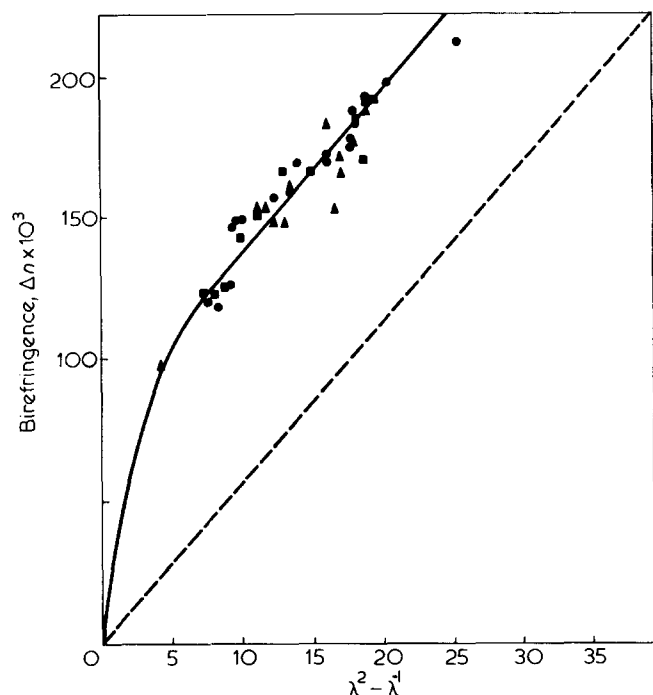


Figure 9 Plot of birefringence $\Delta n \times 10^3$ vs. $\lambda^2 - \lambda^{-1}$. Samples drawn below T_g at 0.125 cm/min. Temperature: ●, 20°C, ■, 40°C, ▲, 60°C, — — — homogeneous draw at 80°C

DISCUSSION

General features of drawing behaviour

We have shown in Figures 3 and 7 that there is a dramatic change in drawing behaviour as the draw temperature is increased through the glass transition range. At low temperatures (less than say 66°C), permanent deformation is localized in a neck, in which the development with strain of molecular orientation (as measured by birefringence) is essentially independent of temperature (and drawing speed⁵). Within each neck there is a systematic variation of strain which evolves as the neck propagates throughout the specimen. In contrast, on drawing at 70°C and above, the strain and birefringence are essentially uniform throughout the specimen, and the increase of birefringence with strain is much more gentle than at lower temperatures. It is of some interest to note that this sudden change with temperature in the mechanism of development of molecular orientation contrasts very markedly with results recently obtained in this laboratory on extruded poly(methyl methacrylate)⁶. In the latter case, there is a gradual change in the mechanism of orientation (and deformation) as the temperature is lowered through the glass transition. At high temperatures the behaviour is typical of a rubber-like material and as temperature is lowered the development of birefringence with extension ratio changes gradually (over approximately 50°C) until at temperatures below 50°C the birefringence—extension ratio curve is reminiscent of the cold drawing curves for PET.

The mechanics of neck formation and propagation are complex as revealed by Figures 4–7. Only certain semi-quantitative aspects of this topic which are relevant to the subsequent analysis may be discussed here. Elements of material on entering the neck deform initially under conditions approximating to pure shear. The high initial elongation in the axial direction occurs at approximately constant width, with concomitant thickness changes maintaining

constancy of volume. These conditions characterize the initiation of a neck and also the situation close to the shoulder of an established neck, where the rapidly deforming material is in both cases effectively constrained by the elastic material outside the neck.

Elements within the neck continue to elongate under the axial stresses but this occurs under conditions which are relaxing more towards the state of simple elongation which is observed at the centre of a long neck. The deformation proceeds with only slight increases in thickness (to a first order, zero) and with substantial reductions in width to maintain constancy of volume; i.e., this second deformation stage also approximates to pure shear but now on an orthogonal plane. Throughout both stages of the deformation, elements near to the edge of the sample experience conditions more nearly of plane stress. These outer elements therefore suffer smaller reductions in thickness, resulting in a transverse section of the neck (perpendicular to the axis) with a profile showing 'pin-cushion' distortion.

Two further aspects need to be mentioned. First, these inhomogeneities in strain are not evident in the birefringence data. It is well-known that a suitable measure of the deformation in the rubbery state to determine the birefringence in the x - y plane is $\lambda_y^2 - \lambda_x^2$. Figures 9 and 10 show that this is also a suitable measure of strain in the glassy state for this purpose. For all the necks studied here $\lambda_y^2 \gg \lambda_x^2$ and therefore small variations in λ_x due to changes between the plane strain and plane stress have only a small effect on $\lambda_y^2 - \lambda_x^2$. The birefringence is therefore essentially dominated by λ_y , which is essentially constant throughout the cold-drawn region. All subsequent data refer to the central section where the conditions most nearly approximate to uniformity of strain and birefringence.

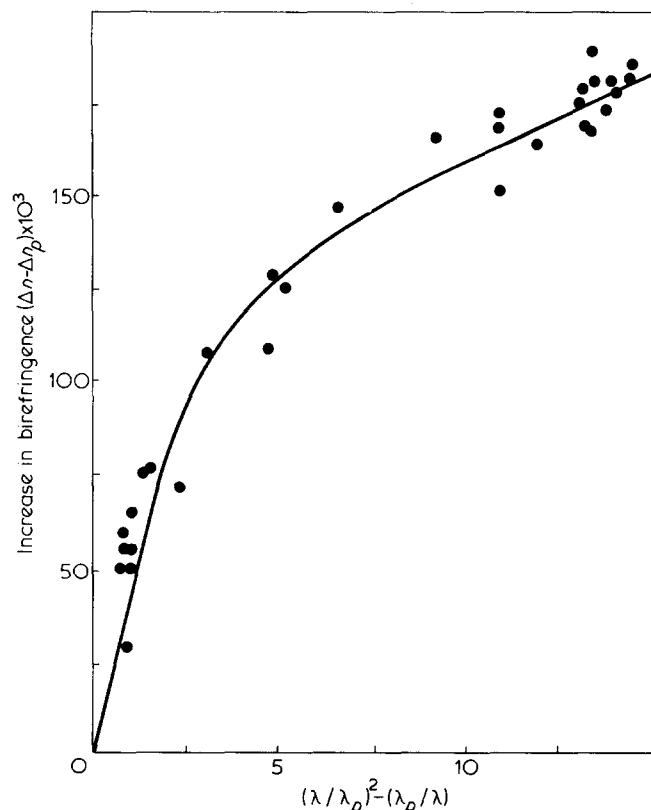


Figure 10 Plot of increase in birefringence in second stage draw $(\Delta n - \Delta n_p) \times 10^3$ vs. $(\lambda/\lambda_p)^2 - (\lambda_p/\lambda)$. λ_p = draw ratio at 80°C, λ = final draw ratio after further drawing at 20°C

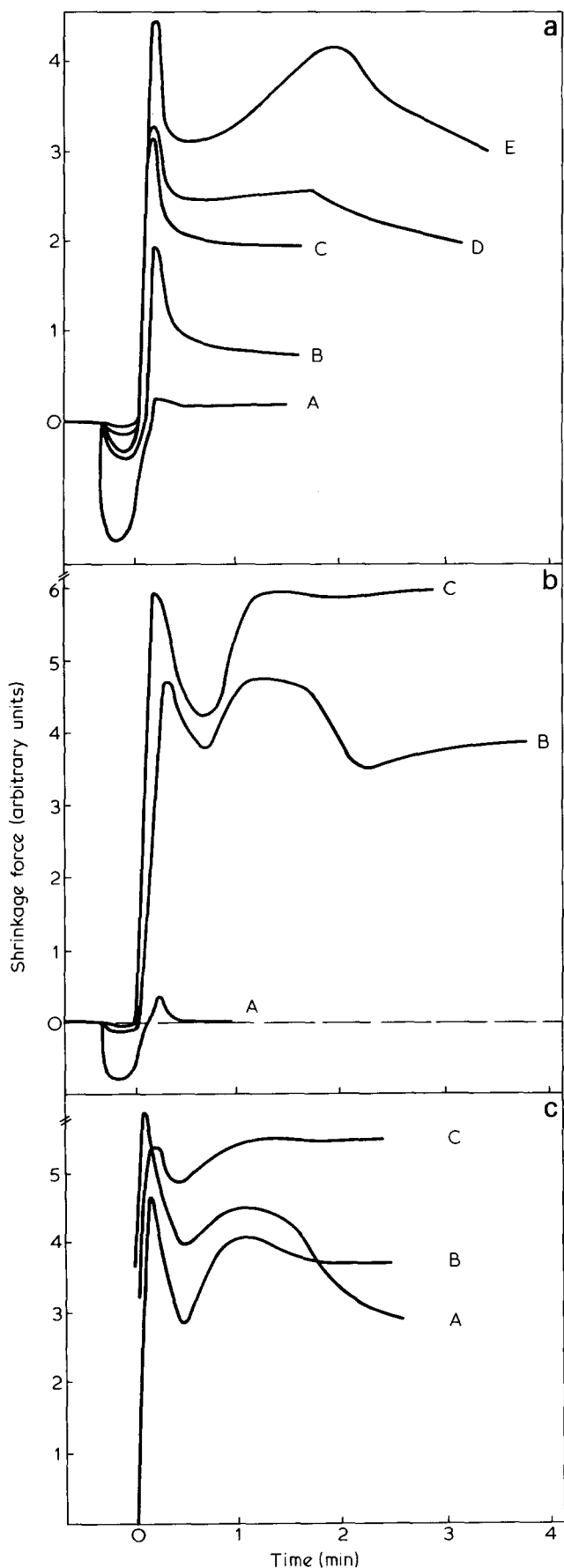


Figure 11 Shrinkage force (arbitrary units) versus time (1 division \equiv 1 min). (a) Samples drawn at 80°C, λ = A, 1.07; B, 1.36; C, 3.4; D, 3.65; E, 3.90. (b) Samples cold drawn at 20°C, A, ΔL = 1.6 mm; B, ΔL = 14 mm; C, ΔL = 25 mm. (c) Two-stage drawn samples, A, λ_p = 1.47, λ = 5.1; B, λ_p = 1.07, λ = 4.07; C, λ_p = 4.2, λ = 5.15

Secondly, as shown in Figure 7, the kinetics of neck growth monitored through the profiles of λ_y and Δ_n at a fixed neck length, ΔL = 12 mm are apparently independent of temperature at temperatures less than say $T_g - 5^\circ\text{C}$ ($T_g \sim 68^\circ\text{C}$ for these specimens). Other data⁵ (not shown here) indicate that the deformation is also relatively strain-rate independent at this range.

Figures 6 and 7 show that both the draw ratio and birefringence of an element increase with increasing time spent in the neck (i.e. with increasing distance from the shoulder). These results are very similar to those obtained for linear polyethylene in another investigation in our laboratory⁷. As in linear polyethylene the drawing process is seen to be time-dependent, although in PET it reaches an identical limit at all temperatures less than, say, $T_g - 5^\circ\text{C}$. These results will be of considerable value below when we come to consider the development of birefringence as a function of deformation ratio.

Hot-drawn material

For uniaxially oriented PET the mean polarizabilities per unit volume \bar{p}_{\parallel} and \bar{p}_{\perp} , parallel and perpendicular to the draw direction, respectively, are given by⁸:

$$\bar{p}_{\parallel} = \frac{1}{3} N(p_1 + p_2 + p_3) + \frac{1}{3} N(2p_3 - p_1 - p_2) \langle P_2(\xi) \rangle \quad (1a)$$

and

$$\bar{p}_{\perp} = \frac{1}{3} N(p_1 + p_2 + p_3) - \frac{1}{6} N(2p_3 - p_1 - p_2) \langle P_2(\xi) \rangle \quad (1b)$$

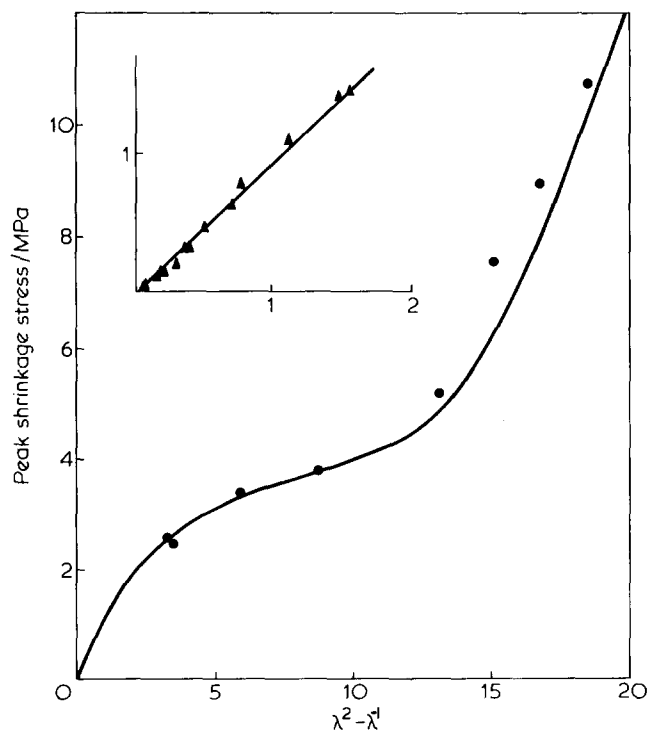


Figure 12 Peak shrinkage stress vs. $\lambda^2 - \lambda^{-1}$ for samples drawn at 80°C at 0.125 cm/min. Inset, data at low extension ratio

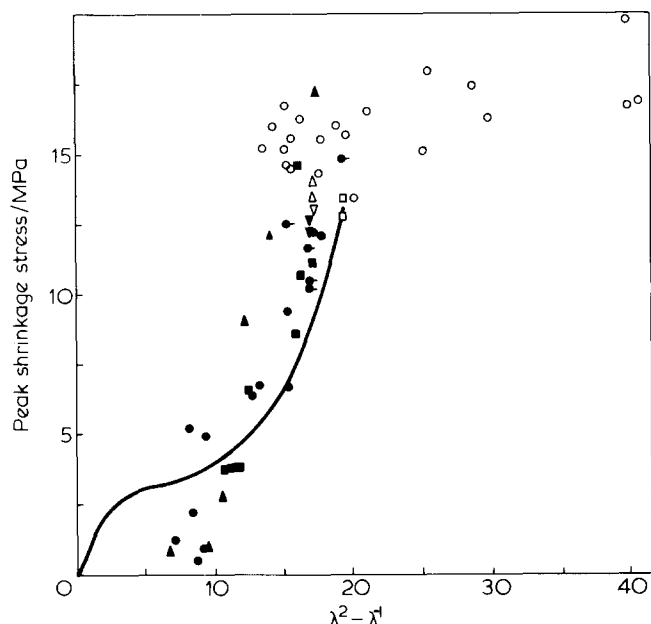


Figure 13 Peak shrinkage stress vs. $\lambda^2 - \lambda^{-1}$ for samples drawn below T_g . Isotropic samples: crosshead speed 0.125 cm/min; $T/^\circ\text{C}$: \bullet , 20; \blacktriangle , 40; \blacksquare , 60. $T = 20^\circ\text{C}$. Speed/cm min $^{-1}$: \triangle , 0.05; \bullet , 0.20; \circ , 0.3; ∇ , 0.5; ∇ , 1.25. Two-stage drawn samples at 0.125 cm/min, \circ , full line from 80°C samples, see Figure 12

p_3 is the polarizability of a structural unit in the chain axis direction, p_2 that at right angles to the chain axis direction but in the plane of the terephthalate residue and p_1 that in the direction perpendicular to both these directions. $P_2(\xi)$ is the second order Legendre polynomial in ξ , which is the cosine of the angle between the draw direction and the axis of a unit of structure (angle brackets denote the ensemble average). N is the number of structural units per unit volume.

Using the Lorentz-Lorenz equation to relate these mean polarizabilities to n_{\parallel} and n_{\perp} , the mean refractive indices parallel and perpendicular to the draw direction, respectively, the birefringence Δn is given by:

$$\Delta n = n_{\parallel} - n_{\perp} = \frac{2\pi(\bar{n}^2 + 2)^2}{9\bar{n}} N \left\{ p_3 - \frac{p_1 + p_2}{2} \right\} \langle P_2(\xi) \rangle \quad (2)$$

where the approximations $n_{\parallel} + n_{\perp} \doteq 2\bar{n}$ and $(n_{\parallel}^2 + 2)(n_{\perp}^2 + 2) = (\bar{n}^2 + 2)^2$ have been made⁹. Since \bar{n} and N are very nearly constant:

$$\Delta n \doteq \Delta n_{\max} \langle P_2(\xi) \rangle \quad (3)$$

where Δn_{\max} is the maximum birefringence of the fully oriented polymer.

For a rubber-like network we identify the structural unit referred to above with the equivalent random link, and theory¹⁰ gives:

$$\langle P_2(\xi) \rangle = \frac{1}{5n} (\lambda^2 - \lambda^{-1}) \quad (4)$$

where n is the number of random links per chain. This expression is valid for small values of $(\lambda^2 - \lambda^{-1})/n$ and corresponds to the Gaussian approximation region of the molecular theory of rubber elasticity⁹. Equation (2) now becomes:

$$\Delta n = \frac{2\pi(\bar{n}^2 + 2)^2}{45\bar{n}} N_0(\alpha_1 - \alpha_2)(\lambda^2 - \lambda^{-1}) \quad (5)$$

where N_0 is the number of chains/unit volume and $(\alpha_1 - \alpha_2)$ is the difference in principal polarizabilities of the random link, [equivalent to the term $\{p_3 - (p_1 + p_2)/2\}$ in equation (2)]. At the same level of approximation the molecular theory of rubber elasticity⁹ shows that the stress is:

$$\sigma = N_0 k T (\lambda^2 - \lambda^{-1}) \quad (6)$$

and that there is a constant stress-optical coefficient

$$C = \frac{\Delta n}{\sigma} = \frac{2\pi(\bar{n}^2 + 2)^2}{45\bar{n}} (\alpha_1 - \alpha_2) \quad (7)$$

The birefringence data from all samples drawn at 80°C are shown in Figure 8 to be linearly dependent on $(\lambda^2 - \lambda^{-1})$ up to $\lambda \sim 4.5$. At first sight, this suggests that the results can be represented by equation (6) over a very wide range of draw ratios. Peak shrinkage stress data, on the other hand, reveal a much more complicated pattern of behaviour (Figure 12). It appears that these data are described by equation (5) only for $\lambda < 1.6$, the region previously studied by stress-optical measurements. The shrinkage stress increases much more slowly in the range $1.6 < \lambda < 3.5$ before a further increase in slope occurs at higher values of λ .

Figure 14 shows the peak shrinkage stress plotted vs. Δn and that the stress-optical coefficient $\Delta n/\sigma$ is a constant as predicted by equation (7) only for small $\lambda < 1.6$; other data¹¹, not presented here, show that the point of departure from linear behaviour depends markedly on the conditions of drawing.

It is interesting to pursue further the analysis of the main data using equations (5) and (6) to calculate from the small λ regions of Figures 8, 13 and 14 values of N_0 and $(\alpha_1 - \alpha_2)$ equal to $1.89 \times 10^{26} \text{ m}^{-3}$ and $1.71 \times 10^{-29} \text{ m}^3$, respectively. These values of the number of chains per unit volume and the polarizability difference of the random link compare very well with the previously published data of Pinnock and Ward¹. It is straightforward to calculate from N_0 that the

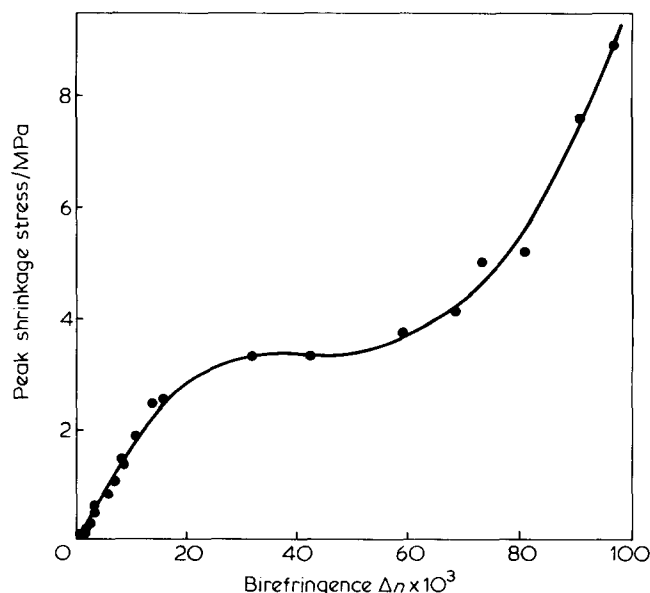


Figure 14 Peak shrinkage stress vs. birefringence, $\Delta n \times 10^3$, samples drawn at 80°C at 0.125 cm/min

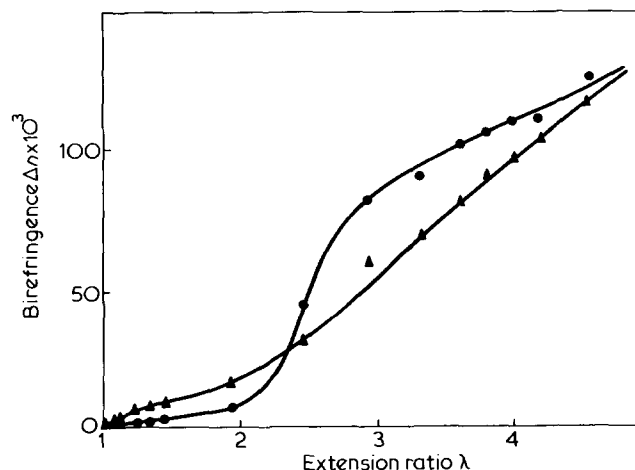


Figure 15 Birefringence versus draw ratio λ (80°C). \blacktriangle , Before; \bullet , after shrinkage force measurements

molecular weight of a chain between entanglements is 4230 which corresponds to approximately 25 monomers per chain. The value of $\alpha_1 - \alpha_2 = 1.7 \times 10^{-29} \text{ m}^3$ for the random link can be compared with values computed for an extended monomer to yield a value of 3.3 monomers/random link and therefore indicating approximately seven random links per chain ($n \sim 7.6$).

The present results for the regions of small λ are consistent with previous studies of orientation in similar samples of PET carried out in our laboratory using the techniques of infra-red dichroism¹², polarized Raman¹³ and fluorescence spectroscopy^{14,15}. The last two techniques have also provided measurements of $\langle P_4(\xi) \rangle$, as well as $\langle P_2(\xi) \rangle$. $\langle P_4(\xi) \rangle$ can also be predicted on the basis of the equivalent random link model¹⁰, giving:

$$\langle P_4(\xi) \rangle = \frac{3}{175n^2} (\lambda^4 - 2\lambda + 1/\lambda^2) + \frac{216}{13475n^3} \left(\lambda^6 - \frac{4\lambda^3}{5} - 7/5 + \frac{6}{5\lambda} \right) + \dots \quad (8)$$

The experimental results for $\langle P_2(\xi) \rangle$ from the present work and for $\langle P_2(\xi) \rangle$ and $\langle P_4(\xi) \rangle$ previously published, where values for $\langle P_4(\xi) \rangle$ are found to be much less than $\langle P_2(\xi) \rangle$, support the general form of equations (5) and (8) at least up to draw ratios of 2.6, confirming that the development of orientation in these materials can be modelled to a good approximation by the deformation of a rubber-like network.

Treloar¹⁶ has derived a more complete expression for $\langle P_2(\xi) \rangle$ based on a good approximation to the inverse Langevin function which is valid to within 1% over the whole range of λ . We have

$$\langle P_2(\xi) \rangle = \frac{1}{5n} (\lambda^2 - \lambda^{-1}) + \frac{1}{150n^2} (\lambda^4 + 2\lambda - 8\lambda^{-2}) + \frac{1}{350n^3} (10\lambda^6 + 6\lambda^3 - 16\lambda^{-3}) \quad (9)$$

As already mentioned, it might appear from Figure 8 that the birefringence data are consistent with the deformation of a rubber-like network up to very high λ . However, consideration of equation (9) in the light of the value

of n of seven obtained from the stress-optical coefficient confirms the result from the shrinkage stress data that the behaviour can only be modelled by a rubber-like network at comparatively low values of λ .

Beyond $\lambda \sim 1.6$ where the shrinkage stress ceases to rise linearly with $(\lambda^2 - \lambda^{-1})$, the shape of the curve is very similar to that generally observed for rubber-like materials. In the region $1.6 < \lambda < 3.5$ where the stress is approximately constant the curve can be modelled by the Mooney–Rivlin equation^{17,18}:

$$\sigma = 2(\lambda^2 - \lambda^{-1}) (C_1 + C_2/\lambda)$$

where $C_1 \sim -5 \times 10^4 \text{ Nm}^{-2}$ and $C_2 \sim 10^6 \text{ Nm}^{-2}$. The physical basis for such analysis has often been questioned¹⁹ and the negative (non-physical) value for C_1 obtained here clearly also casts doubt on the usefulness of the representation. One possible interpretation of these data would be in terms of the breakdown of a limited number of network points in such a way that, although all chains still contribute towards the birefringence, some cease to be effective in supporting stress. The final rise in stress $\lambda \sim 3.5$ is usually attributed to the finite extensibility of the molecular network⁹, which in principle should be modelled through an analogous equation to (9) calculating the stress in terms of the Langevin approximation. It is not clear how such an effect can be evident through the shrinkage stress whilst being undetected through the birefringence.

It is interesting to note that some measure of support for the value of N_0 can also be obtained from the slope of the initial stress–strain curve during drawing at 80°C. The effective modulus obtained yields a value of $N_0 = 2.4 \times 10^{26} \text{ m}^{-3}$ at a drawing speed of $0.125 \text{ cm min}^{-1}$ rising to $9 \times 10^{26} \text{ m}^{-3}$ at a drawing speed of 5 cm min^{-1} . These are encouragingly close to the value of $1.89 \times 10^{26} \text{ m}^{-3}$ obtained from the birefringence and shrinkage stress data, particularly when we recall that the calculations assume explicitly that the shrinkage stress is entirely entropic in origin and can be calculated on the basis of Gaussian statistics.

Finally, it is appropriate to mention the possibility of strain-induced crystallization occurring for the most highly oriented samples studied here. Although crystallization of isotropic PET is negligible at temperatures less than 110°C it has been established that limited crystallization can and does occur at lower temperatures with oriented materials^{15,20–22}. Indications that the ‘as-drawn’ samples do not have an appreciable crystallinity can be obtained from Figure 11 and also from Figure 15 which shows the birefringence versus draw ratio before and after the shrinkage force measurement. Samples with draw ratio less than 2.3 show a reduction in birefringence. This was shown in previous work¹ on samples with comparatively low degrees of preorientation to be simply related, using the stress-optical coefficient, to the decay in shrinkage stress from its maximum value, with a time dependence related to the WLF²³ equation. No evidence of crystallization was found with these samples.

In contrast, samples of high draw ratio ($\lambda > 3.5$) exhibit a second shrinkage force peak (in Figure 11) and an increase in birefringence, both of which may be related to crystallization during the shrinkage force measurement. This suggests that the as-drawn samples are not appreciably crystalline; for $\lambda > 3.5$ crystallization probably occurs at 87°C but only after times which are long compared with those required for the build-up of the entropic shrinkage

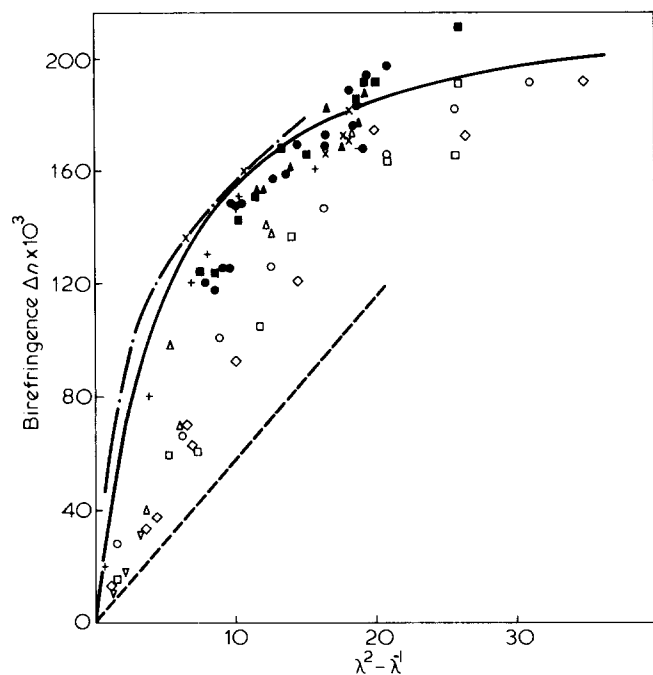


Figure 16 Birefringence vs. $\lambda^2 - \lambda^{-1}$ at different drawing temperatures and rates. Solid symbols $T < T_g$; open symbols $T > T_g$. ●, this work, 20°C; ■, this work, 40°C; ▲, this work, 60°C; —, this work, 80°C. —, Pseudo-affine model, $\Delta n_{\max} = 0.235$. - - -, this work, 2 stage draw. +, Allison and Ward⁴, 2 stage draw; ●, Foot and Ward²⁵, -30°C; X, Foot and Ward²⁵, 20°C; —●, Foot and Ward²⁵, 60°C; ◇, Nobbs, Bower, Ward and Patterson¹⁵, 80°C; □, Cunningham, Ward, Willis and Zichy¹², 80°C; △, Nobbs, Bower and Ward¹⁴, 80°C; △, Nobbs, Bower and Ward¹⁴, 80°C, (partly shrunk); ○, Pinnock and Ward⁸

force. This possibility is presently being studied in our laboratories.

Cold drawn and two-stage drawn materials

Cold drawn and two-stage drawn materials are somewhat similar in properties and together contrast sharply with materials hot drawn at 80°C in two important respects. Consider first the development of birefringence with cold drawing. Figure 9 shows that birefringence increases more rapidly with deformation at temperatures less than the glass transition compared with the rubber-like behaviour seen at 80°C. Raha and Bowden²⁴ obtained similar curves for the development of birefringence in poly(methyl methacrylate) on deformation below its glass transition and suggested that they could be described by equation (6) provided that the constant N_0 was replaced by a function of the strain and the deformation temperature T , viz.

$$N_0(\lambda, T) = N_0(T)e^{-k(T)\lambda}$$

Raha and Bowden suggested that this function modelled the breakdown of entanglements (crosslinks) with deformation and, although Kahar, Duckett and Ward⁶ have shown that this is perhaps not the most likely interpretation of their data, it is interesting to examine its implications with regard to the present data. The initial slope of Figure 9 (and of Figure 10 which shows the two-stage drawn material) is approximately ten times the slope observed for the 80°C data. This would imply that the number of links per chain is now only 7.6/10, i.e. less than one. It is clearly not appropriate to use the rubber network theory under these circumstances and one therefore must

consider the main alternative, i.e. the 'pseudo-affine' deformation scheme. On this scheme, which Ward²⁵ proposed was relevant to the cold drawing of PET, each structural unit rotates as if to follow an imaginary macroscopic line drawn in a homogeneous material but is otherwise undeformed. This 'pseudo-affine' deformation scheme results in a $\langle P_2(\xi) \rangle$ in equation (2) which increases initially much more rapidly with deformation than is described by equation (4), as shown in Figure 16.

Figure 16 shows a comparison between the data from this investigation in relation to previously published data^{4,8,12,14,15,26}. All the present data from samples drawn at room temperature (including two-stage drawn material) together with similar data^{4,26} previously published can be used to define an upper bound curve. This is closely modelled by the 'pseudo-affine' deformation scheme which is shown by a broken line calculated assuming a value for the maximum birefringence $\Delta n_{\max} = 0.235$. By contrast the data from this investigation obtained by drawing at 0.125 cm/min at 80°C (strain rate $\sim 10^{-4} \text{ sec}^{-1}$) apparently provided a lower bound (which may not be an absolute bound but no data with a higher draw temperature or lower draw speed are available at present). In between these two bounds lie data from previous publications^{8,12,14,15} obtained by drawing PET at 80°C at a comparatively higher speed (e.g. a strain rate $\sim 3 \times 10^{-2} \text{ sec}^{-1}$ was used for samples drawn over a pin as described by Nobbs *et al.*¹⁵). Those data from samples drawn at higher speeds are also linear in $\lambda^2 - \lambda^{-1}$, at least for moderate values of λ , and so can be described by equation (2) with a higher value of N_0 ; this reflects perhaps the larger number of physical entanglements effective at the higher speeds. It would appear therefore that subject to the reservations discussed in relationship to the birefringence data in the previous section, the data can be modelled by a rubber network using equation (2) at low draw ratios, followed by a transition to the pseudo-affine scheme at higher draw ratios. This is brought on perhaps by the complete extension of certain network chains which then merely rotate towards the draw direction and slip through the physical entanglements. A transition to the pseudo-affine scheme occurs immediately on drawing below T_g .

It is not possible to consider only the birefringence data when discussing deformation schemes which must also be consistent with the shrinkage stress data shown in Figures 12–14. As the shrinkage stress behaviour is qualitatively different for the cold drawn and two-stage drawn material it is appropriate at this stage to discuss previous proposals for the structure of these materials. Ward²⁵ proposed that on cold drawing, each unit of the structure (random link) rotates towards the draw direction according to the pseudo-affine deformation scheme. Because the units are inextensible this necessarily involves a certain amount of slip between units – a process which continues until a limiting deformation called the natural draw ratio is reached. It was shown that this natural draw ratio was approximately independent of temperature below T_g but was very sensitive to any preorientation introduced in the spinning process⁴, and this led Ward to postulate the idea of a limiting extension of a network. These ideas receive support from the present data in two ways.

(1) The total draw ratio achieved in the two-stage process is effectively independent of λ_p , the draw ratio in the 80°C stage, as shown in Figure 17. However, there is a substantial statistical variation in the total draw ratio. Note that the range of preorientation studied here is much greater

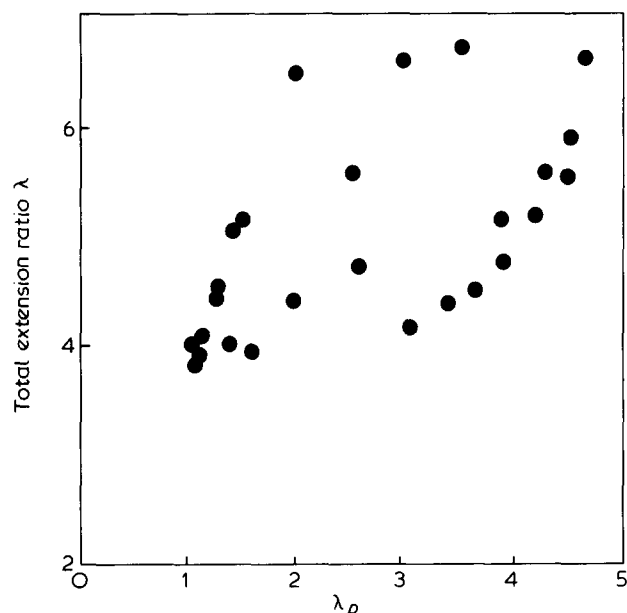


Figure 17 Total draw ratio λ as a function of preorientation draw-ratio λ_p

than that in previous studies where λ was less than 1.4.

(2) The increase in birefringence in newly formed necks (not previously studied in detail) is described adequately by the 'pseudo-affine' deformation scheme. The shrinkage stress, however, is negligible in these specimens until the birefringence approaches its maximum value (Figure 13). For these highly oriented specimens the shrinkage stress increases steeply with increasing deformation to lie consistently higher than similar data for hot drawn material. Continuity between the cold drawn and two-stage drawn materials is established for $\lambda \sim 4$ and thereafter the shrinkage stress increases more slowly with increasing λ .

The tentative picture which emerges from these experiments is complex. Drawing of isotropic or preoriented specimens at temperatures below T_g involves a comparatively rapid development of orientation of the structural units. In the initial stages of neck growth this orientation is not associated with a large shrinkage stress which is only observed for specimens approaching their limiting draw ratio. Samples with a relatively high limiting draw ratio show a shrinkage stress which is slightly higher.

Finally, it must be noted that the low shrinkage stresses measured with cold drawn materials were obtained with samples containing very narrow necks, $\Delta L \sim 1-2$ mm. The method of shrinkage force measurement used here inevitably introduced a systematic error tending to underestimate the true shrinkage stress. Further work is in progress in an attempt to avoid these errors in a very difficult measurement.

CONCLUSIONS

Studies of the deformation behaviour of PET as a function of temperature show that the transition from cold drawing through a neck to homogeneous deformation occurs in a narrow temperature range between 60° and 80°C at the glass transition temperature of the polymer T_g .

The homogeneous deformation above 80°C is consistent

with the deformation of a molecular network in the rubbery state, although the stress-optical properties show divergence from the simple Gaussian statistical theory for deformation ratios greater than ~ 1.7 .

Below 60°C, the cold drawing behaviour is independent of temperature and strain rate to a good approximation. It appears that the development of molecular orientation in the early stages of the cold drawing deformation does not involve cooperative molecular rearrangements. The orientation can therefore be very well modelled by the pseudo-affine deformation scheme which assumes the independent orientation of units of structure (in this case probably monomer units in the molecular chain). When cold drawn samples of low deformation ratio are heated above T_g , the shrinkage forces are apparently very small, consistent with the view that there has been no great change in the overall topology of the molecular chains. For high deformation by cold drawing, however, samples subsequently show shrinkage forces comparable to and even larger than those obtained by drawing above 80°C. This suggests that a molecular network is then involved and is consistent with the previous proposal that the limit of deformation for such samples (the natural draw ratio) is determined by the limiting extensibility of a molecular network.

REFERENCES

- 1 Pinnock, P. R. and Ward, I. M. *Trans. Faraday Soc.* 1966, **62**, 1308
- 2 Marshall, I. and Thompson, A. B. *Proc. Roy. Soc. (A)* 1954, **221**, 541
- 3 Allison, S. W., Pinnock, P. R. and Ward, I. M. *Polymer* 1966, **7**, 66
- 4 Allison, S. W. and Ward, I. M. *Br. J. Appl. Phys.* 1967, **18**, 1151
- 5 Rietsch, F. unpublished results
- 6 Kahar, N., Duckett, R. A. and Ward, I. M. *Polymer* 1978, **19**, 136
- 7 Capaccio, G., Crompton, T. A. and Ward, I. M. *J. Pol. Sci. (Polym. Phys. Edn)* 1976, **14**, 1641
- 8 Pinnock, P. R. and Ward, I. M. *Br. J. Appl. Phys.* 1964, **15**, 1559
- 9 Treloar, L. R. G. 'The Physics of Rubber Elasticity' Clarendon Press, Oxford, 1958
- 10 Roe, R. J. and Krigbaum, W. R. *J. Appl. Phys.* 1964, **35**, 2215
- 11 Bower, D. I., Korybut, K., Nobbs, J. H. and Ward, I. M. to be published
- 12 Cunningham, A., Ward, I. M., Willis, H. A. and Zichy, V. *Polymer* 1974, **15**, 749
- 13 Purvis, J. and Bower, D. I. *J. Polym. Sci. (Polym. Phys. Edn)* 1976, **14**, 1461
- 14 Nobbs, J. H., Bower, D. I. and Ward, I. M. *Polymer* 1976, **17**, 25
- 15 Nobbs, J. H., Bower, D. I., Ward, I. M. and Patterson, D. *Polymer* 1974, **15**, 287
- 16 Treloar, L. R. G. *Trans. Faraday Soc.* 1954, **50**, 881
- 17 Mooney, M. J. *J. Appl. Phys.* 1940, **11**, 582
- 18 Rivlin, R. S. *J. Appl. Phys.* 1948, **18**, 444
- 19 Treloar, L. R. G. *Proc. Roy. Soc. (A)* 1976, **351**, 301
- 20 Smith, F. S. and Steward, R. D. *Polymer* 1974, **15**, 283
- 21 Wilson, M. P. W. *Polymer* 1974, **15**, 277
- 22 Bhatt, G. M. and Bell, J. P. J. *Polym. Sci. (Polym. Phys. Edn)* 1976, **14**, 575
- 23 Williams, M. L., Landel, R. F. and Ferry, J. O. *J. Am. Chem. Soc.* 1955, **77**, 370
- 24 Raha, S. and Bowden, P. B. *Polymer* 1972, **13**, 174
- 25 Ward, I. M. *Proc. Phys. Soc.* 1962, **80**, 1176
- 26 Foot, J. S. and Ward, I. M. *J. Mater. Sci.* 1975, **10**, 955